Theory of magnetic edge states in chiral graphene nanoribbons

Oleg V. Yazyev,[1,2] Rodrigo B. Capaz,[1,3] and Steven G. Louie[1,2]
[1]*Department of Physics, University of California, Berkeley, California 94720, USA*
[2]*Materials Sciences Division, Lawrence Berkeley National Laboratory, Berkeley, California 94720, USA*
[3]*Instituto de Física, Universidade Federal do Rio de Janeiro, Caixa Postal 68528, Rio de Janeiro, RJ 21941-972, Brazil*
(Received 20 June 2011; published 9 September 2011)

Using a model Hamiltonian approach including electron-electron interactions, we systematically investigate the electronic structure and magnetic properties of chiral graphene nanoribbons. We show that the presence of magnetic edge states is an intrinsic feature of smooth graphene nanoribbons with chiral edges, and discover a number of structure-property relations. Specifically, we study the dependence of magnetic moments and edge-state energy splittings on the nanoribbon width and chiral angle as well as the role of environmental screening effects. Our results address a recent experimental observation of signatures of magnetic ordering in chiral graphene nanoribbons and provide an avenue toward tuning their properties via the structural and environmental degrees of freedom.

DOI: 10.1103/PhysRevB.84.115406 PACS number(s): 73.22.Pr, 73.20.−r, 75.75.−c

I. INTRODUCTION

Graphene and derived nanostructures exhibit a large number of novel electronic properties.[1–3] One of such features is the presence of electronic states localized at the edges of this two-dimensional (2D) nanomaterial.[4] These zero-energy edge states were predicted to give rise to a novel type of magnetic ordering[5] that may lead to practical carbon-based magnetic materials.[6] Even more appealing is the prospective of realizing the theoretical proposals of novel spintronic devices based on graphene.[7–11] While evidence for edge states has been seen experimentally,[12,13] no solid proof of edge magnetism in graphene was presented until now.

A recent scanning-tunneling microscopy/spectroscopy (STM/STS) study of graphene nanoribbons (GNRs) with ultrasmooth edges showed the presence of edge states with characteristic splitting in the dI/dV spectra—an unambiguous indication of magnetic ordering.[14] These GNRs, produced by the chemical unzipping of carbon nanotubes,[15] are chiral, i.e., characterized by low-symmetry orientation of the edges rather than by high-symmetry zigzag and armchair directions. While the presence of edge states at the chiral graphene edges is broadly recognized,[4,16–18] theoretical investigations of magnetic ordering driven by electron-electron (e-e) interactions have so far focused only on zigzag edges.

In this paper, we systematically study the electronic structure of chiral GNRs using a self-consistent model Hamiltonian approach including e-e interactions. In particular, we investigate GNRs characterized by a broad range of chiralities and widths as well as address the effects of varying e-e interaction strength. Our study reveals that spin-polarized edge states are an intrinsic feature of chiral GNRs, in agreement with the recent experimental observations. Moreover, we find a number of structure-property relations and unambiguous signatures of magnetic ordering of edge states, which opens new prospectives for their further exploration and for developing practical spintronic devices based on them.

The present paper is organized as follows. In Sec. II, we describe computational methods and structural models of chiral GNRs used in our work. Section III first presents the results of tight-binding calculations, and then discusses the results of calculations involving e-e interactions. Section IV concludes our work.

II. COMPUTATIONAL METHODS

The method employed in our study is based on the mean-field approximation to the Hubbard Hamiltonian

$$\mathcal{H} = -t \sum_{\langle i,j\rangle,\sigma} [c^\dagger_{i\sigma} c_{j\sigma} + \text{H.c.}] + U \sum_i (n_{i\uparrow}\langle n_{i\downarrow}\rangle + \langle n_{i\uparrow}\rangle n_{i\downarrow} - \langle n_{i\uparrow}\rangle\langle n_{i\downarrow}\rangle). \quad (1)$$

The first term is the nearest-neighbor tight-binding Hamiltonian in which $c_{i\sigma}$ ($c^\dagger_{i\sigma}$) annihilates (creates) an electron with spin σ at site i, $\langle i,j\rangle$ stands for the nearest-neighbor pairs of atoms, and $t \sim 3$ eV.[3] The second term accounts for e-e interactions. The expectation values of the spin-resolved density $n_{i\sigma} = c^\dagger_{i\sigma} c_{i\sigma}$ depend on the eigenvectors of $\mathcal{H}$. Thus a self-consistent field procedure is used for solving the problem. We assume the magnitude of the on-site Coulomb repulsion parameter is comparable to the magnitude of hopping integral t ($U/t \sim 1$). Our choice of U/t is justified by the experimental studies of neutral soliton states in *trans*-polyacetylene–a one-dimensional (1D) sp^2 carbon system equivalent to a zigzag GNR of the smallest possible width—from which $U \approx 3.0$ eV has been obtained.[19,20] The assumed magnitude of U/t is further corroborated by the values of U deduced from first-principles calculations based on density functional theory.[21–23] However, we point out that this effective parameter may incorporate environmental factors such as the enhancement of screening due to the proximity of dielectric or metallic substrate.[14] For this reason, we also study the dependence of results on the magnitude of on-site Coulomb repulsion by considering $U/t = 0.5, 1.0, 1.5$. The mean-field approximation was shown to be accurate for the considered range of magnitudes of U/t.[24,25]

Two parameters determine the structure of smooth GNRs: (i) the crystallographic direction of the edge and (ii) the width. In general, the direction of the nanoribbon's edge is defined by some translation vector (n,m) of the graphene lattice. For

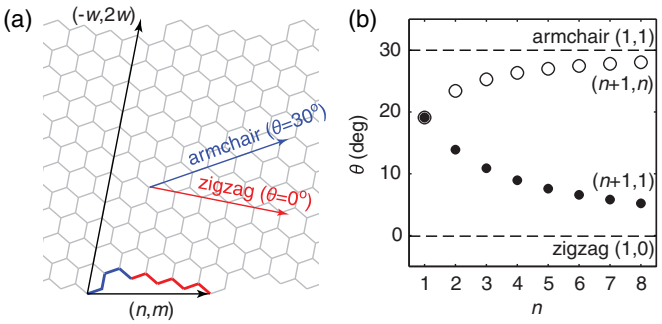

FIG. 1. (Color online) (a) Atomic structure of a model of chiral graphene nanoribbon. The structure shown corresponds to $\theta = 10.9^\circ$ chiral GNR characterized by edge repeat vector (4,1) and width $w = 6$. Zigzag and armchair units of the edge are indicated. (b) Chirality angles θ of the considered $(n+1,1)$ and $(n+1,n)$ series of chiral GNRs.

high-symmetry zigzag and armchair edges, these vectors are (1,0) and (1,1), respectively. Since graphene edges specified by (n,m) and (m,n) are structurally equivalent, we present here results for edges with $n > m$. The edge of (n,m) nanoribbon is a repeating structure composed of $n - m$ zigzag units and m armchair units as illustrated for the particular case of a (4,1) GNR in Fig. 1(a). In our work, we have not considered possible reconstructions of graphene edges and assume that the undercoordinated edge atoms are terminated by simple functional groups with electronegativity similar to the one of carbon (e.g., hydrogen atoms). The length of repeat vector $a = \overline{(n,m)} = a_0\sqrt{n^2 + nm + m^2}$, where $a_0 = 0.246$ nm is the lattice constant of graphene. Alternatively, chirality can be described by the chirality angle

$$\theta = \arcsin\sqrt{\frac{3}{4}\left(\frac{m^2}{n^2 + nm + m^2}\right)}. \qquad (2)$$

Zigzag and armchair edges are characterized by $\theta = 0^\circ$ and $\theta = 30^\circ$, respectively, while for chiral edges $0^\circ < \theta < 30^\circ$. We consider chiral GNRs defined by edge translational vectors $(n+1,1)$ and $(n,n+1)$ $(n \geqslant 1)$. These two series cover the whole range of chirality angles θ and converge to $\theta = 0^\circ$ and 30°, respectively, with increasing n [see Fig. 1(b)]. The configurations of chiral GNRs considered in this study cover $4.7^\circ < \theta < 25.3^\circ$. The width $W = \sqrt{3}wa_0\cos\theta$ of a GNR is defined by vector $(-w,2w)$ pointing along the armchair direction as shown in Fig. 1(a).

III. DISCUSSION OF RESULTS

A. Tight-binding model results

We start our discussion by considering the evolution of tight-binding band structures of GNRs (neglecting *e-e* interactions, $U/t = 0$) upon the change of chirality from zigzag ($\theta = 0^\circ$) to armchair ($\theta = 30^\circ$) via the series of intermediate chiral configurations at fixed nanoribbon width ($w = 12$). High-symmetry zigzag nanoribbon [see Fig. 2, left panel] exhibits a flat band at the Fermi level ($E = 0$), which spans one-third of the 1D Brillouin zone (BZ), that is, the corresponding density of edge states per edge length per spin $\rho(\theta = 0^\circ) = 1/(3a_0)$. Armchair GNRs [see Fig. 2, right panel] are either metals or semiconductors with no electronic states localized at the edges. This result can be rationalized within the infinite-width picture by considering the 2D band structure of graphene projected onto the 1D BZ of periodic edge.[26] In the case of an armchair GNR, both Dirac points (K and K') of graphene's band structure are projected onto the Γ point of 1D BZ. However, for a zigzag GNR, points K and K' are projected onto $k = 2\pi/(3a)$ and $k = -2\pi/(3a)$, respectively, with a zero-energy flat band connecting these two points [see Fig. 2, insets]. The band structures of chiral GNRs in the infinite-width limit can be obtained by continuous rotation of the band structure of graphene which leads to the known result[16]:

$$\rho(\theta) = \frac{2}{3a_0}\cos\left(\theta + \frac{\pi}{3}\right). \qquad (3)$$

That is, in the limit of large width, only armchair GNRs show no edge states. The density of edge states is largest for zigzag nanoribbons and shows almost linear dependence on θ. The tight-binding band structures of $w = 12$ chiral GNRs (see Fig. 2; the x axis scales correspond to the 1D BZ dimensions) confirm this picture. Two important comments should be made: (i) in finite-width GNRs with edge orientation close to the armchair direction, zero-energy edge states are partially or even completely suppressed, and (ii) in GNRs with edge orientation close to the zigzag direction, the flat edge-state

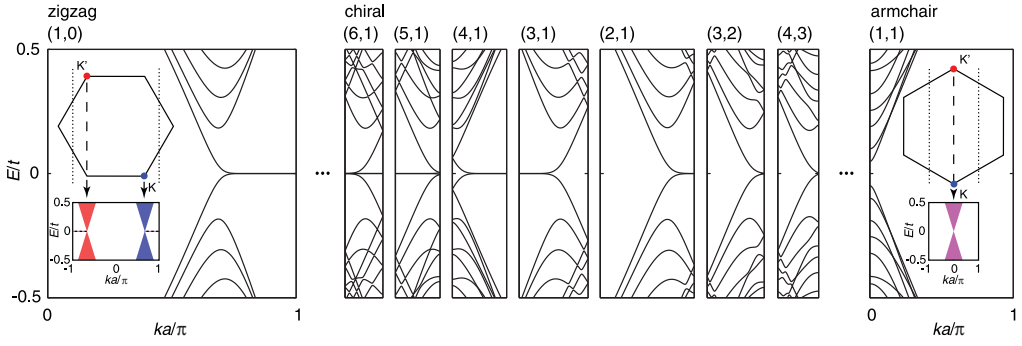

FIG. 2. (Color online) Evolution of the tight-binding band structures (no *e-e* interactions) of graphene nanoribbons ($w = 12$) upon the change of chirality from zigzag ($\theta = 0^\circ$) to armchair ($\theta = 30^\circ$) via the series of intermediate chiral configurations. The scales of the plots account for the varying Brillouin-zone dimensions. The insets schematically illustrate the projection of points K and K' of the 2D BZ of ideal graphene onto the 1D band structures of zigzag and armchair GNRs.

band spans the whole 1D BZ and becomes multiple degenerate due to band folding.

B. Mean-field Hubbard model results

We now discuss the effects of *e-e* interactions on the electronic spectra of chiral GNRs. Figure 3(a) shows the band structure and the density of states (DOS) plot for a zigzag GNR ($w = 12$) obtained within the mean-field Hubbard model ($U/t = 1$) compared to the tight-binding results ($U/t = 0$). In the presence of *e-e* interactions, the electronic ground state of the zigzag GNR exhibits an interesting magnetic ordering: ferromagnetic (FM) along the edges and antiferromagnetic (AFM) across the nanoribbon.[5] The magnetic moment per edge unit length $M = 0.313\ \mu_B/a_0$. Spin-polarization lifts the degeneracy of edge states and opens an electronic band gap Δ^0. While the tight-binding DOS has only one van Hove singularity related to the presence of 1D edge states at $E = 0$, the mean-field Hubbard model solution shows two pairs of peaks split by Δ^0 and Δ^1. We note that Hamiltonian (1) respects electron-hole symmetry. The presence of band gap Δ^0 is related to the AFM correlation between the opposite edges, while the larger splitting Δ^1 is due to the FM correlation along one single edge of most strongly localized electronic states at $k = \pi/a$.[7,28,29] Thus the presence of band gap Δ^0 and splitting Δ^1 constitute independent signatures of magnetic ordering across the nanoribbon and along its edge. The rest of electronic spectrum ($|E| > 0.18t$) is negligibly affected by the Hubbard term. Van Hove singularities at $|E| \approx 0.2t$ and higher energies correspond to the bulklike states subjected to quantum confinement in 1D GNRs of the given width. The mean-field Hubbard model electronic spectra of chiral GNRs show all the features characteristic of zigzag GNRs provided the ground state is spin polarized. Both splittings, especially Δ^1, are reduced in the case of (2,1) GNR ($\theta = 19.1°$) due to the smaller magnetic moment $M = 0.096\ \mu_B/a_0$ [see Fig. 3(b)]. Nanoribbons with chirality close to $\theta = 0°$ show additional pairs of van Hove singularities due to splittings of the multiple degenerate edge-state bands at $k = 0$ and $k = \pi/a$ [see Fig. 3(c) for $\theta = 7.6°$ (6,1) GNR]. Figure 3(d) shows the distribution of spin density in

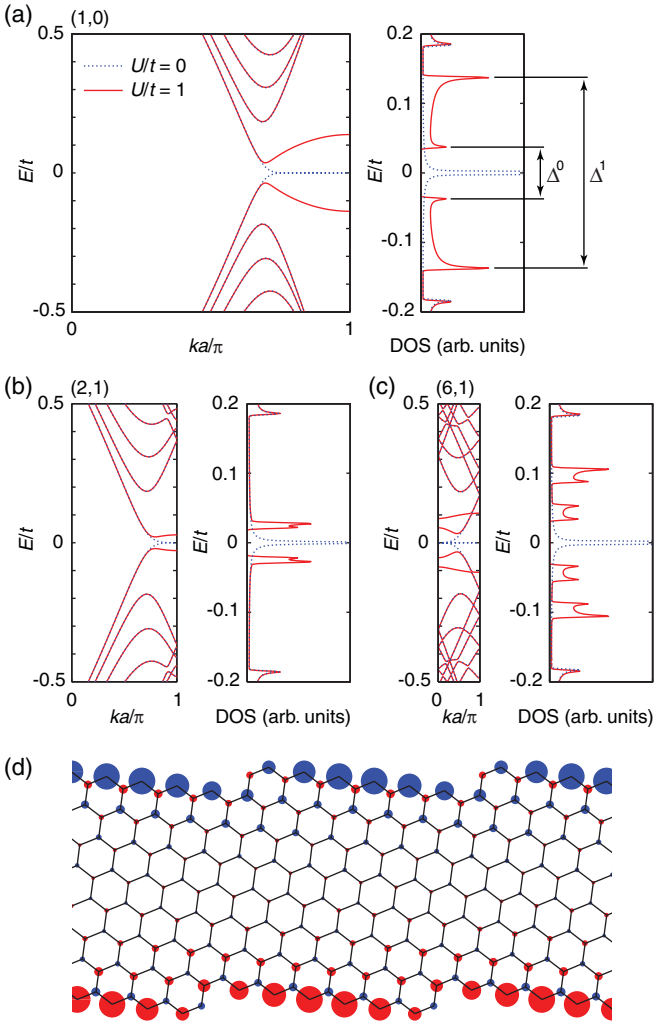

FIG. 3. (Color online) (a) Effects of the electron-electron interactions on the band structure (left panel) and the density of states (right panel) of a zigzag GNR ($w = 12$). Dashed and solid curves correspond to the tight-binding model ($U/t = 0$) and the mean-field Hubbard model ($U/t = 1$), respectively. (b) and (c) Respective band structure and density-of-states plots for (2,1) and (6,1) chiral GNRs. (d) Spin-density distribution in (6,1) chiral GNR ($w = 4$). Circle areas correspond to the local magnetic moments from the mean-field Hubbard model solution obtained at $U/t = 1$.

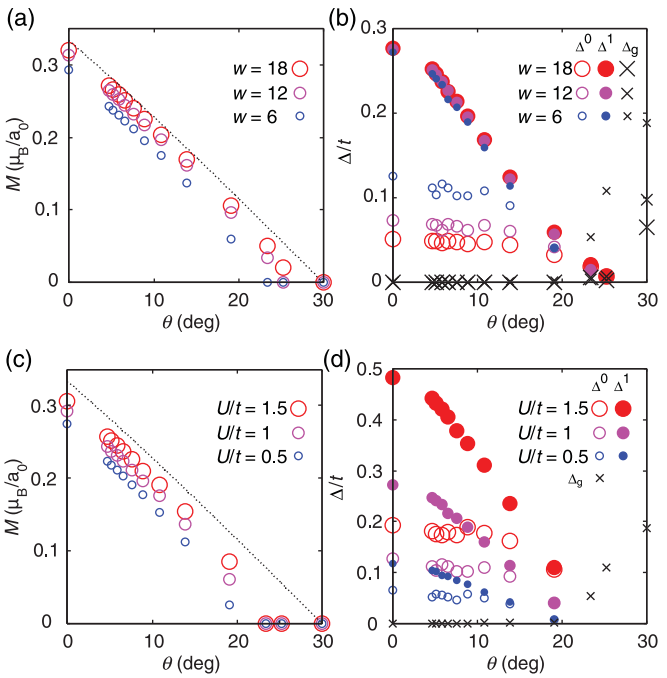

FIG. 4. (Color online) (a) Magnetic moment per edge unit length M as a function of chirality angle θ for three different nanoribbon widths w from the mean-field Hubbard model ($U/t = 1$) calculations. The dotted line shows magnetic moments in the limit of infinite width [see Eq. (3)]. (b) Electronic band gap Δ^0 and maximum energy splitting Δ^1 as a function of θ for different values of w (mean-field Hubbard model, $U/t = 1$). Crosses indicate the tight-binding band gaps Δ_g. The values of (c) M and (d) Δ^0 and Δ^1 obtained using the mean-field Hubbard model at different values of U/t and $w = 6$.

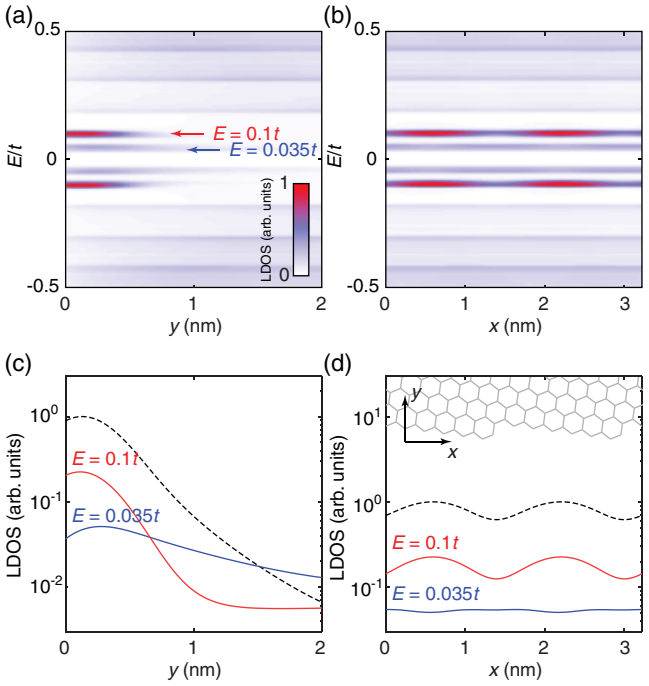

FIG. 5. (Color online) Variation of the local density of states (LDOS) (a) across the (6,1) chiral GNR (x axis is oriented along the edge, $y = 0$ corresponds to the outermost edge atom) and (b) along its edge obtained using the mean-field Hubbard model ($U/t = 1$). (c) and (d) Log-linear plots of LDOS at the energies indicated in panel (a) across the (6,1) chiral GNR and along its edge, respectively. The dashed lines correspond to the tight-binding LDOS at $E = 0$. The inset in panel (d) superimposes the edge structure with the plot.

(6,1) GNR ($w = 4$) obtained using the mean-field Hubbard model at $U/t = 1$. Similarly to the case of zigzag GNRs, local magnetic moments are mostly localized on the edge atoms. However, the illustration also reveals the modulation of spin-density distribution along the edge. The magnetic moments are mostly localized on the zigzag segments of chiral edge while spin density is largely suppressed at the armchair segments.

Figure 4 summarizes the calculated magnetic moments and energy splittings for GNRs of various chiralities and widths, and different magnitudes of U/t. At $U/t = 1$, spin-polarized ground states of few-nm-wide GNRs span almost full range of chiralities [see Fig. 4(a)]. The magnetic moments per unit length M follow closely the dotted curve that corresponds to the complete spin-polarization of edge states in the infinite-width limit (3), but appear to be negatively shifted by nearly constant amounts that are moderately dependent on width. Splitting Δ^1 shows a similar dependence on θ and it is independent of w [see Fig. 4(b)]. On the contrary, the magnitude of Δ^0 is largely insensitive to the variations of θ in broad ranges of this parameter, but shows a clear dependence on w analogous to the case of zigzag GNRs.[27] This is in good agreement with the STM/STS data obtained for several GNRs of different chiralities and widths.[14] As the chiral angle θ approaches 30°, magnetic moments vanish and the tight-binding band gaps Δ_g quickly rise reaching their maximum values for the corresponding armchair GNRs.[30]

Figure 4(c) reveals a moderate dependence of $M(\theta)$ on the strength of e-e interactions while the magnitudes of Δ^0 and Δ^1 are both approximately proportional to U/t [see Fig. 4(d)]. Such a behavior can be understood by the fact that even weak e-e interactions are able to trigger a complete spin polarization of the zero-energy edge states thus leading to a direct relation between the magnetic moments and the density of edge states. However, the magnitudes of splittings Δ^0 and Δ^1 are also related to the magnitude of the spin-dependent potential, which depends on U/t.

Finally, we turn our attention to the spatial variation of electronic spectra of magnetic graphene edges in relation to the experimental observations.[14] As a case study, we investigate the mean-field Hubbard model ($U/t = 1$) local density of states (LDOS) evaluated across the (6,1) chiral GNR ($w = 12$, $W = 5$ nm) [see Fig. 5(a)] and along its edge [see Fig. 5(b)]. We find that both pairs of contributions to the total DOS due to the edge states seen in Fig. 3(c) are localized at the edge. However, the higher-energy LDOS peak at $E = 0.1t$ decays very fast being confined within the 1-nm-wide edge region while the lower-energy feature at $E = 0.035t$ penetrates deep into the middle of GNR. The series of peaks at $E \gtrsim 0.2t$ repeated in energy by $\approx 0.1t$ correspond to the bulklike graphene states subjected to quantum confinement. The total density of edge states from the tight-binding calculations shows pronounced oscillations along the GNR edge [dashed curve in Fig. 5(d)]. The oscillation period corresponds to the edge periodicity $a = 1.6$ nm. The $E = 0.1t$ LDOS peak from the mean-field Hubbard model follows this trend. In contrast, the lower-energy peak ($E = 0.035t$) shows weak variations of LDOS. This behavior was found to be generic to all studied chiral and zigzag magnetic GNRs.

IV. CONCLUSIONS

To summarize, our model Hamiltonian investigation showed that the presence of magnetic edge states is an intrinsic feature of smooth graphene nanoribbons with chiral edges. The study also revealed a number of structure-property relations such as the dependence of magnetic moments and edge-state energy splittings on the nanoribbon width and chiral angle. The described relations can serve as spectroscopic signatures of edge-state magnetism in graphene nanoribbons and provide an avenue toward controlling magnetic and electronic properties of these nanostructures.

ACKNOWLEDGMENTS

We would like to thank C. Tao, M. F. Crommie, and Y.-W. Son for discussions. This work was supported by NSF Grant No. DMR10-1006184 (numerical simulations of GNRs) and by the Director, Office of Science, Office of Basic Energy Sciences, Division of Materials Sciences and Engineering Division, US Department of Energy under Contract No. DE-AC02-05CH11231 (software development of electron correlation effects). R.B.C. acknowledges support from Brazilian agencies CNPq, CAPES, FAPERJ, and INCT Nanomateriais de Carbono and the ONR MURI program. Computational resources have been provided by NSF through TeraGrid facility at NICS (Kraken).

[1] A. K. Geim and K. S. Novoselov, Nat. Mater. **6**, 183 (2007).
[2] M. I. Katsnelson, Materials Today **10**, 20 (2007).
[3] A. H. Castro Neto, F. Guinea, N. M. R. Peres, K. S. Novoselov, and A. K. Geim, Rev. Mod. Phys. **81**, 109 (2009).
[4] K. Nakada, M. Fujita, G. Dresselhaus, and M. S. Dresselhaus, Phys. Rev. B **54**, 17954 (1996).
[5] M. Fujita, K. Wakabayashi, K. Nakada, and K. Kusakabe, J. Phys. Soc. Jpn. **65**, 1920 (1996).
[6] *Carbon-Based Magnetism: An Overview of Metal Free Carbon-Based Compounds and Materials*, edited by T. Makarova and F. Palacio (Elsevier, Amsterdam, 2005).
[7] Y.-W. Son, M. L. Cohen, and S. G. Louie, Nature (London) **444**, 347 (2006).
[8] O. V. Yazyev and M. I. Katsnelson, Phys. Rev. Lett. **100**, 047209 (2008).
[9] M. Wimmer, İ. Adagideli, S. Berber, D. Tománek, and K. Richter, Phys. Rev. Lett. **100**, 177207 (2008).
[10] F. Muñoz-Rojas, J. Fernández-Rossier, and J. J. Palacios, Phys. Rev. Lett. **102**, 136810 (2009).
[11] O. V. Yazyev, Rep. Prog. Phys. **73**, 056501 (2010).
[12] Y. Kobayashi, K.-i. Fukui, T. Enoki, K. Kusakabe, and Y. Kaburagi, Phys. Rev. B **71**, 193406 (2005).
[13] Y. Kobayashi, K.-i. Fukui, T. Enoki, and K. Kusakabe, Phys. Rev. B **73**, 125415 (2006).
[14] C. Tao, L. Jiao, O. V. Yazyev, Y.-C. Chen, J. Feng, X. Zhang, R. B. Capaz, J. M. Tour, A. Zettl, S. G. Louie, H. Dai, and M. F. Crommie, Nat. Phys. **7**, 616 (2011).
[15] L. Jiao, X. Wang, G. Diankov, H. Wang, and H. Dai, Nat. Nanotechnology **5**, 321 (2010).
[16] A. R. Akhmerov and C. W. J. Beenakker, Phys. Rev. B **77**, 085423 (2008).
[17] M. Wimmer, A. R. Akhmerov, and F. Guinea, Phys. Rev. B **82**, 045409 (2010).
[18] W. Jaskólski, A. Ayuela, M. Pelc, H. Santos, and L. Chico, Phys. Rev. B **83**, 235424 (2011).
[19] S. Kuroda, H. Bando, and H. Shirakawa, Solid State Commun. **52**, 893 (1984).
[20] H. Thomann, L. R. Dalton, M. Grabowski, and T. C. Clarke, Phys. Rev. B **31**, 3141 (1985).
[21] L. Pisani, J. A. Chan, B. Montanari, and N. M. Harrison, Phys. Rev. B **75**, 064418 (2007).
[22] D. Gunlycke, D. A. Areshkin, J. Li, J. W. Mintmire, and C. T. White, Nano Lett. **7**, 3608 (2007).
[23] O. V. Yazyev, Phys. Rev. Lett. **101**, 037203 (2008).
[24] H. Feldner, Z. Y. Meng, A. Honecker, D. Cabra, S. Wessel, and F. F. Assaad, Phys. Rev. B **81**, 115416 (2010).
[25] H. Feldner, Z. Y. Meng, T. C. Lang, F. F. Assaad, S. Wessel, and A. Honecker, Phys. Rev. Lett. **106**, 226401 (2011).
[26] O. V. Yazyev and S. G. Louie, Nat. Mater. **9**, 806 (2010).
[27] Y.-W. Son, M. L. Cohen, and S. G. Louie, Phys. Rev. Lett. **97**, 216803 (2006).
[28] J. Fernández-Rossier, Phys. Rev. B **77**, 075430 (2008).
[29] J. Jung, T. Pereg-Barnea, and A. H. MacDonald, Phys. Rev. Lett. **102**, 227205 (2009).
[30] M. Ezawa, Phys. Rev. B **73**, 045432 (2006).